Marijan Marković[1], Zvonimir Petranović[2], Milan Vujanović[1]

Numerical Simulation of Asynchronous E-motor with Field-Circuit Coupling

[1]Faculty of Mechanical Engineering and Naval Architecture, University of Zagreb, Zagreb, Croatia
[2]AVL List GmbH, Graz, Austria

Abstract

The focus of this work is a comparative analysis of two numerical methods for asynchronous electric motor simulations. Magnetic potential formulation is employed in each method separately, using Ansys Maxwell for finite element method and AVL FIRE M for finite volume method. 2D simulations are conducted on a Siemens squirrel cage induction motor validating the simulation results on the datasheet information form the manufacturer. Although axial symmetry is exploited for a 2D approach, 3D effects of a rotor cage are considered coupling the field and circuit equations. End ring resistance and inductance are fed directly into the solver which has been proven to increase the accuracy of the results from the regular 2D approach and is feasible in both methods. Torque results for both methods incorporating field-circuit coupling show discrepancies of less than 5% compared to the data from the manufacturer. Conversely, simulations omitting field-circuit coupling show higher torque discrepancies of more than 10%. Two initialization strategies are used to demonstrate the superior speed of the torque output with frequency domain initialization compared to the steady state case. Numerical results show excellent agreement between the numerical simulations and the data from the manufacturer. Also, convergence time is investigated varying mesh sizes for the finite volume method. Finally, it is shown that a faster convergence time is achieved employing the finite element method mainly since it was running with a coarser mesh not containing boundary layers.

Keywords: *Squirrel cage induction motor; magnetic potential; 2D simulations; finite volume method; frequency domain simulation*

1. Introduction

Electrification of the transport sector in the last decades has sparked the development and research of electric motors. It is well established that numerical analysis of electrical machinery is the essential tool in the field of electrical engineering. Regarding the market representation, the most prevailing motor in the world is still the squirrel cage induction motor (SCIM), due to its simplicity and robustness, making it a subject of design optimization and performance evaluation in the engineering community.

The industry standard for the analysis of electromagnetic phenomena in electric machines is the Finite Element Method (FEM). Numerous FEM-based software packages have been employed to perform electromagnetic simulations enabling engineers to predict the behavior of SCIMs [1]. These simulations provide valuable insights into motor performance under different operating conditions and aid in the design and optimization process. FEM-based simulations are also used as a starting point for prototyping and testing of electric motors for electric vehicles applications, reducing the price of the design process [2]. Due to a good accuracy-computational efficiency trade-off, 2D electromagnetic analysis is often employed on radial machines instead of a full-scale 3D analysis [3]. Moreover, field results gathered from a 2D geometry simulation can be used as an input for a thermal analysis accounting for electromagnetic losses as heat sources in thermal analysis [4]. To increase the accuracy of a 2D FEM model, 3D effects are considered via field-circuit coupling [5]. Herein, stator winding and rotor cage end regions are modelled by resistance and inductance circuit elements [6]. Such coupled models are employed in time-stepping finite element analysis to calculate stator and rotor core hysteresis losses [7]. Regarding the time discretization of a 2D FEM field-circuit model, time-periodic finite element method can be employed to reduce computational effort compared to a classical time-stepping method [8]. Moreover, additional 3D effects such as radial ventilation ducts can be considered through use of equivalent permeability in stator and rotor cores, accounting for permeabilities of air and steel separately [9].

While FEM is the go-to numerical method for electric machinery simulations, researchers have been exploring alternative methods with comparable accuracy and computational efficiency. Here, Finite Volume Methods (FVM) comes in play as an established method in computational fluid dynamics and increasingly applied in electromagnetic simulations in recent years. FVM has been employed to simulate the behavior of an induction motor in 2D geometry on a test case from COMPUMAG conferences i.e., TEAM problem 30a [10]. Obtained results are in good agreement with analytical results confirming the accuracy of the method [11]. Further development of FVM for SCIM applications in 2D geometry was undertaken by Petranović et al. to couple the external circuit and field equations for rotor bars currents, incorporating 3D effects of a short-circuited squirrel cage rotor in a 2D model [12]. Rotor end ring currents are directly coupled with magnetic potential field equation through potential gradient term i.e., voltage, which leads to an altered system matrix. The influence of additional terms is practically included in the simulation assigning the amount of end ring inductance and resistance. Recent development of finite volume framework for SCIM applications has raised the question of this approach comparability with the traditional finite element framework.

On that account, 2D analysis of a three-phase squirrel cage induction motor with external circuit coupling is

conducted employing two different numerical approaches. Finite element analysis is conducted using Ansys Maxwell, while the finite volume analysis uses AVL's Fire M. Both software packages are using $\vec{A}$-Φ formulation to describe electric and magnetic fields which is an advantage regarding the comparability of methods. To the best of the author's knowledge, there haven't been any publications regarding 2D simulations of SCIM with field-circuit coupling applied on an existing SCIM in the finite volume framework. Therefore, this paper is focused on investigating a real Siemens SCIM employing a 2D approach with field-circuit coupling offering a possibility of results validation on the data from the manufacturer. Both methods are using transient simulations, assisted with frequency/eddy current solutions for shorter initialization time, and a more rapid convergence. Transient simulations with steady state initialization are also conducted to show the influence of initialization techniques on convergence time. Complexity of use and computational efficiency are compared for both methods and mesh sensitivity analysis is conducted.

2. Model assumptions and equations

Before the equation overview, some model assumptions and clarifications are stated here.

1. All simulations carried out in the scope of this paper are in 2D geometries spanning the x-y plane on a radial machine which implies the following. Current density vector and magnetic potential vector both have only one component which is in z direction. Similarly, magnetic flux density and field intensity have components in x and y direction.
2. Eddy effects are omitted in both stator and rotor cores considering the lamination of both parts. Stacking factor is equal to one.
3. Stator edge effects are neglected and modelled with zero magnetic potential boundary condition.
4. 3D effects are considered only in rotor accounting for the end ring resistance and inductance coupling the field equations with external circuit equations. Stator winding 3D effect are not considered.

Field equation solved numerically is derived expressing Ampère's circuital law through magnetic vector potential. Quasistatic equation omitting the displacement current term in $\vec{A} - \Phi$ formulation is defined in (1).

$$\nabla \times \frac{1}{\mu}(\nabla \times \vec{A}) = \sigma\left(-\frac{\partial \vec{A}}{\partial t} \nabla\Phi + \vec{v} \times (\nabla \times \vec{A})\right) \tag{1}$$

The double curl term on the left-hand sign can be rewritten as diffusion term, while the right-hand side amounts to a current source density term and a total time derivative encompassing a partial derivative of and a motional term for the induced current calculation as show in (2).

$$\nabla \cdot \frac{1}{\mu}(\nabla \vec{A}) = \sigma\left(-\frac{d\vec{A}}{dt} - \nabla\Phi\right) \tag{2}$$

$-\nabla\Phi$ term is not explicitly calculated but is instead imposed as a source current density in the stator winding to describe the differences in electric potential. $-\nabla\Phi$ term in rotor bars is used to couple the field-circuit equations, but electric potential is once again not explicitly solved. Therefore, electric potential calculation is not explicitly calculated anywhere in discretized space. Instead, rotor bar current in 2D geometry exists because of a changing magnetic flux density (magnetic potential), to which the $-\nabla\Phi$ term is contributing through end ring inductance and resistance. v×(∇×A) term is present in the rotor domain which is separated from stator domain at the half distance of air gap length.

Since this work also encompasses frequency domain solution initialization, an equation for this solution type is given in (3). Unlike the transient simulations, which are solved in multiple time steps using backwards Euler to discretize the time derivative, field equations are solved in a single step like magnetostatic simulations. The difference is that here, magnetic vector potential is solved in a complex space assuming harmonic magnetic field due to harmonic source excitations. Field equation then looks like:

$$\nabla \cdot \frac{1}{\mu_{eff}}(\nabla \vec{A}_C) = \sigma\left(-j\omega\vec{A}_C - \nabla\Phi_C + \vec{v} \times (\nabla \times \vec{A}_C)\right) \tag{3}$$

Where μ_{eff} is an effective permeability, and ω is an angular frequency [13]. $\vec{A}_C$ and Φ_C are complex values of a magnetic and electric potential written through their real and imaginary part as:

$$\vec{A}_C = \vec{A}_R + j\vec{A}_I \tag{4}$$

$$\Phi_C = \Phi_R + j\Phi_I \tag{5}$$

In the finite volume approach used by Fire M, equations (1) and (3) are discretized in time and space occupied by mesh consisting of finite volumes. Magnetic potential equation is then solved for each finite volume yielding the value of magnetic potential in the center of the volume i.e., approach is cell centered. Conversely, the finite element approach employed by Ansys Maxwell for solving the Ampère's equation is edge/node based using tetrahedra/triangles for space discretization [14]. Ansys Maxwell employs the first order edge elements for the magnetic vector potential and second order nodal elements for the electric potential. Magnetic potential in one finite element is defined as:

$$\vec{A} = \sum_{k=1}^{Ne} a_k \vec{N}_k \tag{6}$$

where a_k is the circulation of the magnetic potential along a finite element edge, and $\vec{N}_k$ is the edge shape function associated with kth edge. $\vec{N}_k$ is defined as:

$$\vec{N}_k = n_n \nabla n_m - n_m \nabla n_n \tag{7}$$

3. Induction Motor Design

The electric motor chosen for software comparison is an asynchronous 36/26 Siemens motor with squirrel cage rotor. Electrical data is acquired from the manufacturer's datasheet [15]. Motor geometry is measured from the actual motor and drawn in CAD-software which is used to feed the meshers of both software. Important geometrical and electrical data are shown in table 1.

Table 1. *Geometrical and electrical data*

Geometrical data		Electrical data	
Outer stator diameter	125 mm	Rated power	0.75 kW
Rotor diameter	75 mm	Rated speed	1395 rpm
Shaft diameter	32 mm	Rated torque	5.1 Nm
Air gap length	1 mm	Frequency	50 Hz
Axial length	70 mm	Rated current	1.88 A (VY)
Stator slots	36	Number of phases	3
Number of strands	91	End ring inductance	$4.7 \cdot 10^{-9}$ H
Rotor slots	26	End ring resistance	$1.565 \cdot 10^{-6}\,\Omega$

End ring resistance and inductance are calculated analytically and used as an input in both software [16].

The value of phase resistance necessary for end ring resistance calculation is computed assuming the rotor bar temperature to be 75 °C. Calculated resistance is subsequently used to couple the external circuit of the rotor edge with field equations. Motor layout is shown in Fig. 1.

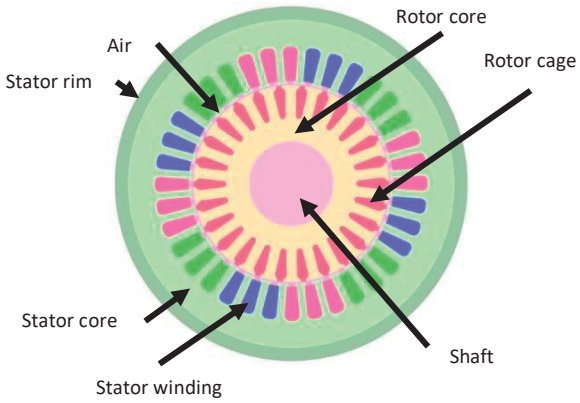

Fig. 1. Induction motor layout

4. Mesh and Numerical Setup Mesh

Once all the necessary geometrical data is acquired, 2D meshes are generated in both software. Tetrahedral Mesh in Ansys Maxwell is on a 2D sheet, while Fire M uses a different approach due to the finite volume-based formulation which requires a physical volume to discretize the space. This is achieved by having a one cell depth in the 3rd dimension, so the mesh technically has an arbitrary long third dimension. Meshes are shown in figure 2.

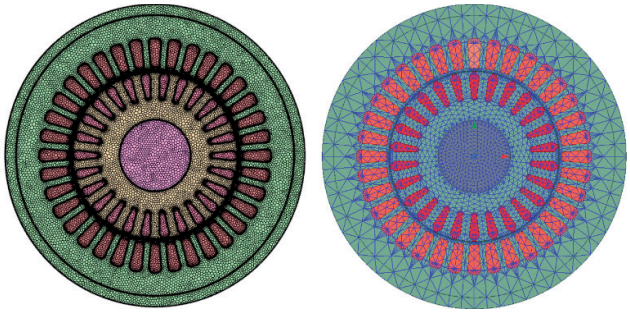

Fig. 2. Computational mesh: Fire M (left), Ansys Maxwell (right)

It is apparent that Maxwell is using a much smaller mesh consisting of 8780 tetrahedral elements, while the mesh in Fire M is consisted of 91562 cells, most of which are polyhedral. Finite element mesh is much smaller since Maxwell uses proprietary adaptive mesh refinement algorithms by default, which are automatically designed to detect and refine the mesh in regions with the largest field error. The mesh is initially created for the magnetostatic case using the adaptive refinement with the energy error parameter set to 1% and after that fed to the transient simulation [14]. Regarding the complexity of use, it is important to state that both software come with automated tools for mesh and model assembly requiring minimal input of geometrical and electric data, which also generate the meshes. The software then takes advantage of axial symmetry and solves only half the domain reducing computational effort. However, in this case, author created the full mesh by hand, employing the default setup from each software. Taking the movement of rotor into account, special care needs to be taken when creating the mesh in Fire M which uses a more complex approach opposed to Ansys Maxwell. Here, rotor and stator need to be physically disjointed in the middle of the airgap to allow for the use of mesh deformation formula which manages the rotation of each rotor cell in a time-marching scheme [17]. Note: Mesh deformation is just the name of the utility in Fire M which is in charge of mesh manipulation by user. Since the cell nodes in the air gap, although identically positioned are disjointed, no mesh deformation takes place. Instead, only the rotation is occurring. On the other hand, Ansys Maxwell uses the motion band feature to set up rotation of the rotor which is applied to a circle in the airgap previously assigned during geometry manipulation. Rotational speed is kept constant amounting to 1395 revolutions per minute.

Time dependency

Both software run transient simulations with a duration of 1 second and a time step of 1 millisecond, or 1000 time steps. When considering the sinusoidal dependence

of winding sources with phase angle shifts for the B and C phase, source terms setup in both approaches is quite similar. Furthermore, the excitation method used employs stranded configuration, which ignores the eddy effects (skin and proximity effects) in the winding domain. The only domain where the eddy effects are calculated is the rotor bars because electrical steel lamination also causes them to be ignored in the rotor and stator core.

Boundary conditions

Boundary conditions are the same in both software with the default boundary condition on every multi-material interface where the direction of the magnetic field is prescribed in equation 8. The outer edge of the domain surrounded by air has the zero magnetic potential prescribed as $\vec{A} = (0,0,0)$.

$$\vec{n} x \vec{H} = \vec{0} \tag{8}$$

Initial conditions

Two different simulations are run to highlight the significance of proper initialization from the perspective of the initial conditions. To provide the solver with the magnetic potential result in the first simulation, steady state initial conditions were used. The frequency/eddy current solver is used in the second simulation as the initial solution in the zeroth time step. Simulations converge much faster than in the steady state initialization case, demonstrating significant time savings for the same configuration because the frequency solver also calculates induced current in the rotor bars.

Solver and other differences

The two software also differ in the type of solver used for calculating the linearized system of equations. Ansys Maxwell uses a direct solver by default, while Fire M employs an iterative solver, in this case a generalized minimal residual. The relative residual tolerance for an iterative solver is set to . Solution obtained from the direct solver is considered as an exact solution within the limits of numerical precision.

Frequency/eddy current solver

Instead of using the moving mesh with a sinusoidal excitation, slip frequency and phase angles are assigned to the winding domain. Slip frequency is set as =3.5 Hz and the phase angles are set to 0° for phase A, 120° for phase B, and 240° for phase C.

5. Result analysis

Displayed results are divided in two parts. Firstly, steady state initialization results are presented alongside the simulation time and mesh sensitivity analysis. After that, frequency domain initialization is shown.

Steady state initialization

Regarding the steady state initialization, it takes the simulations at least 20 stator electrical periods to approach the steady state value. Convergence plot of torque values for both software is shown in figure 3. Curves are almost identical and follow the same trend with a minor peak in value in the beginning of simulation. Simulations are carried out in no load condition.

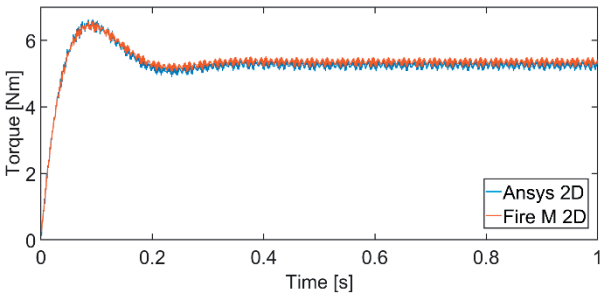

Fig. 3. Torque convergence, steady state initialization

Averaged values over the last two stator electrical periods are shown in table 2 and compared with a reference torque. Results overshoot the reference value by approximately 5%. Values of torque obtained with exact simulations in table 2, but without end ring coupling are shown to emphasize the importance of rotor edge effects. Discrepancies are undershooting the reference value by 10%.

Table 2. *Torque results*

	Datasheet	**Fire M**	**Ansys Maxwell**
Torque with end ring	5.1 Nm	5.34 Nm	5.27 Nm
Torque without end ring	-	4.68 Nm	4.65 Nm

Field plots for magnetic potential and magnetic flux density are shown in figures 4 and 5. It is apparent they are almost in perfect agreement.

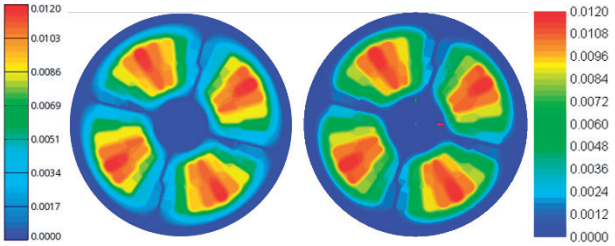

Fig. 4. Magnetic potential field: Fire M (left), Ansys Maxwell (right)

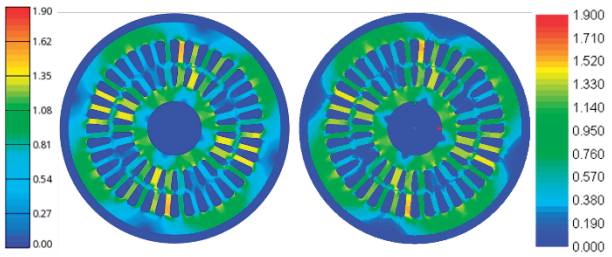

Fig. 5. Magnetic flux density field: Fire M (left), Ansys Maxwell (right)

Considering rotor bars are the only domain where eddy effects are calculated, induced current from an arbitrary rotor bar is examined and compared between the two software. Results are shown in figure 6. Once again, the curves are almost overlapping verifying the validity of an alternative finite volume approach.

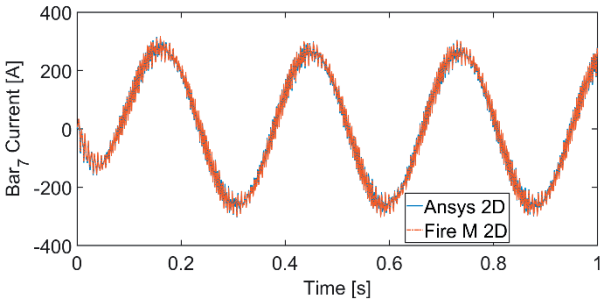

Fig. 6. Induced current in Rotor bar 7, steady state initialization

Simulation Time

For comparability purposes, both simulations incorporating steady state initialization with initial meshes are run on 4-CPUs on an Intel Xeon CPU E4-2650 processor. According to expectations, Fire M simulation on a much larger mesh takes longer to complete. One of the reasons is the use of boundary layer as a default setup in 2D polymesher which substantially increases the number of cells. Therefore, a mesh sensitivity analysis is carried out generating 3 additional meshes with fewer cells. Comparison of CPU time is shown in table 3.

Table 3. *Computational time comparison*

	Average WCT	Torque
Ansys Maxwell	45 min	5.27 Nm
Fire M - 91562	169.1 min	5.34 Nm
Fire M - 48970	127.3 min	5.33 Nm
Fire M - 32908	119 min	5.36 Nm
Fire M - 12015	80.2 min	5.17 Nm

Reducing the mesh size in finite volume approach by factor of 8 has decreased the computational time by a factor of 2 with limited impact on the accuracy of solution. Torque in the smallest mesh shows minor difference considering no boundary layers are used in the air gap where the torque is calculated. Induced current shape in smaller meshes is also well described. It is important to state that both software have output all available field plots for each time step which has increased the simulation time significantly. This is once again done for comparability purposes since Ansys Maxwell integrates the current density over the surface of a rotor bar to get a plot shown in figure 6. Incorporating that additional time for results output, makes the total time to 62 minutes. On the other hand, this time is incorporated into Fire M's WCT, since the user needs to manually add all integral results and field plots necessary for results evaluation before the simulation. This just proves simulation time heavily depends on the wanted output result, which makes it difficult to properly compare simulation time from both methods. Comparing the smallest polyhedral mesh with tetrahedral mesh gives similar accuracy, with slightly higher computational time. Therefore, it is concluded that employing a coarse mesh in finite volume approach offers a viable alternative for 2D approach for SCIM numerical analysis.

Frequency domain initialization

Initialization with frequency domain solver offers the advantage of faster convergence to a steady state solution compared to steady state initialization approach. Main cause of this is the consideration of the induced currents in rotor bars, which in turn give different results of the magnetic field and subsequently, magnetic potential. Figure 7 shows the comparison of current density field in frequency/eddy current solver. It is noticeable that induced currents are homogenous within each rotor bar.

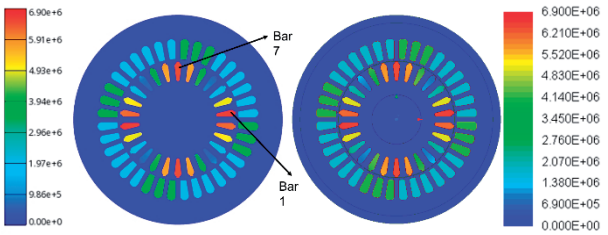

Fig. 7. Current density field: Fire M (left), Ansys Maxwell (right)

Comparison of calculated torques and induced currents in selected bars is shown in table 4. Results are in very good agreement and the discrepancies are almost non-existent. Torque prediction is very close to the reference value from the manufacturer with a discrepancy of less than 4%.

Table 4. *Frequency domain results*

	Ansys Maxwell	Fire M
Torque	5.30 Nm	5.29 Nm
Bar 1 Current	265.53 A	265.45 A
Bar 7 Current	-260.71 A	-259.92 A

Once the simulations in the frequency domain are finished, results for the magnetic potential are fed to the transient solver in a similar manner for both software. Simulations are also run for 1 s. Figure 8 shows the convergence of frequency/eddy current initialization compared to a steady state initialization. It is shown that convergence of both transient solvers is very similar to each other with small discrepancy following the trend from steady state initialization convergence. It is also apparent that the simulation converges in the first few time steps so the end time of the simulation beyond this comparison could be significantly reduced depending on the wanted output quantity.

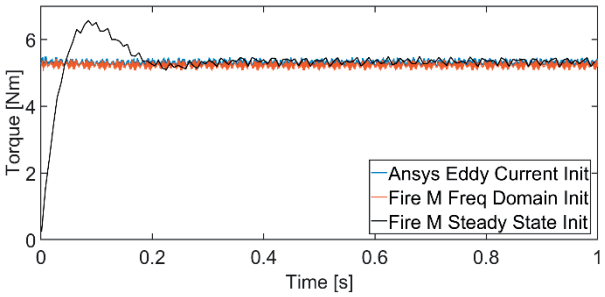

Fig. 8. Torque convergence, frequency domain initialization

Figure 9 shows the convergence of the same bar current as figure 6, but with frequency initialization. It is visible that the current is starting from the values shown in table 4., unlike the steady state initialized solution where the current starts from zero. Overall computational time is almost identical to steady state approach for 1000 timesteps (excluding the short time it takes the frequency solver to converge), but in practice can be shortened. To describe a one electrical period of a rotor bar current it is sufficient to run the simulation for 0.286 seconds in which time this motor makes more than 6 revolutions around its axis for the current slip frequency.

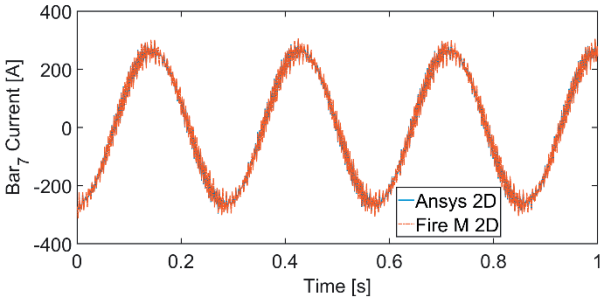

Fig. 9. Induced current in rotor bar 7, frequency domain initialization

6. Conclusion

Finite element and finite volume method performance are compared analyzing the behavior of a squirrel cage induction motor employing commercial software. Ansys Maxwell and Fire M show almost identical results for relevant field quantities, as well as for torque, which is in good agreement with the reference value deviating less than 5 %. Mesh sensitivity analysis has shown that similar computational time can be achieved in both software when the finite volume mesh is coarsened by removing boundary layers from the mesh with minor influence on accuracy. Moreover, the frequency and the quantity of output results for a time-marching scheme heavily influence the computational time which can be doubled if the fields are written for every time step. Although exact comparability of computational time is hard to assess due to the fundamental differences between FEM and FVM, Ansys Maxwell still offers 30% faster converges for similar load when comparing the coarsest finite volume mesh with finite element mesh. However, this percentage is influenced by the file output frequency and the difference between direct and iterative solver operations. Regarding the complexity of use, Ansys Maxwell has proven to be faster to use and more user friendly, but Fire M allows for more user control e.g., linear solver tolerance, underrelaxation parameters manipulation and has better overview of the solver performance. Furthermore, frequency domain initialization has proven to significantly decrease the calculation time opposed to steady state initialization. Torque output from the frequency domain solver is sufficient even without the subsequent transient analysis and has less than 4% discrepancy with reference value. If the complete field results for every rotor angle position are required, computational time can be shortened running the simulation for one rotor electrical period. Future work will be reserved for the expansion of the current 2D model to incorporate the stator edge effect within the FVM simulations.

Acknowledgment

This work has been supported by the Croatian Science Foundation. This work has been supported by the Horizon Europe project INITIATE (ID: 101136775). This support is gratefully acknowledged.

7. References

[1] Ahmadi M, Poshtan J, Poshtan M. Modelling squirrel cage induction motors using finite element method. 2012 IEEE International Conference on Intelligent Control, Automatic Detection and High-End Equipment, IEEE; 2012, p. 186–91. https://doi.org/10.1109/ICADE.2012.6330124.

[2] De Gennaro M, Jürgens J, Zanon A, Gragger J, Schlemmer E, Fricassè A, et al. Designing, prototyping and testing of a ferrite permanent magnet assisted synchronous reluctance machine for hybrid and electric vehicles applications. Sustainable Energy Technologies and Assessments 2019;31:86–101. https://doi.org/10.1016/j.seta.2018.12.002.

[3] Ferkova Z. Comparison between 2D and 3D Modelling of Induction Machine Using Finite Element Method. Advances in Electrical and Electronic Engineering 2015;13. https://doi.org/10.15598/aeee.v13i2.1346.

[4] Li L, Yu Q, Jiang Z, Liu Y, Guo M. Thermal-electromagnetic coupling simulation study of high efficiency and energy saving application of induction motor for offshore oil platform. Energy Reports 2021;7:84–9. https://doi.org/10.1016/j.egyr.2021.02.019.

[5] De Gersem H, Hameyer K, Weiland T. Field–circuit coupled models in electromagnetic simulation. J Comput Appl Math 2004;168:125–33. https://doi.org/10.1016/j.cam.2003.05.008.

[6] Savov VN, Georgiev ZhD, Bogdanov ES. Analysis of cage induction motor by means of the finite element method and coupled system of field, circuit and motion equations. Electrical Engineering 1997;80:21–8. https://doi.org/10.1007/BF01235666.

[7] Wan X, Li Y, Zhang C, Yang Q, Zhu J. Field-circuit coupled T-S finite element analysis of core losses for induction motor. 2017 20th International Conference on Electrical Machines and Systems (ICEMS), IEEE; 2017, p. 1–4. https://doi.org/10.1109/ICEMS.2017.8056340.

[8] Xiaoyan Wang, Dexin Xie. Analysis of Induction Motor Using Field-Circuit Coupled Time-Periodic Finite Element Method Taking Account of Hysteresis. IEEE Trans Magn 2009;45:1740–3. https://doi.org/10.1109/TMAG.2009.2012802.

[9] Aragón Verduzco DA, Escarela Pérez R, Olivares Galván JC, Campero Littlewood E, Maximov S, Hernández Ávila JL. Numerical simulation of a squirrel cage motor including magnetic wedges and radial vents. Ingeniería Investigación y Tecnología 2021;22:1–10. https://doi.org/10.22201/fi.25940732e.2021.22.4.025.

[10] https://www.compumag.org/jsite/images/stories/TEAM/problem30a.pdf n.d.

[11] Benghalia R, Cheriet A, Amrani I. The Finite Volume Method an Alternative Method for LF Electromagnetic Problems. European Journal of Electrical Engineering 2020;22:301–11. https://doi.org/10.18280/ejee.224-507.

[12] Petranovic Z, Santner S, Urthaler P, Fink C. Numerical simulation of squirrel cage induction machine. 2021 IEEE Vehicle Power and Propulsion Conference (VPPC), IEEE; 2021, p. 1–6. https://doi.org/10.1109/VPPC53923.2021.9699128.

[13] “AVL FIRE M User Manual.” GmbH, AVL List, Graz, 2023. n.d.

[14] “ANSYS Maxwell User Manual.” ANSYS Inc., Canonsburg, PA, USA, 2022. n.d.

[15] https://mall.industry.siemens.com/mall/en/WW/Catalog/Product/1LA70834AA10 n.d.

[16] Asad B, Vaimann T, Kallaste A, Rassolkin A, Belahcen A. Winding Function Based Analytical Model of Squirrel Cage Induction Motor for Fault Diagnostics. 2019 26th International Workshop on Electric Drives: Improvement in Efficiency of Electric Drives (IWED), IEEE; 2019, p. 1–6. https://doi.org/10.1109/IWED.2019.8664314.

[17] “AVL FAME M User Manual.” GmbH, AVL List, Graz, 2023. n.d